Analysis of Structural Transformations during the Synthesis of a MoVTeNb Mixed Oxide Catalyst

P. Beato[a], A. Blume[a], F. Girgsdies[a], R. E. Jentoft[a], R. Schlögl[a], O. Timpe[a],

A. Trunschke[a], G. Weinberg[a]

[a]Fritz Haber Institut der Max Planck Gesellschaft, Faradayweg 4-6, 14195 Berlin,

Germany

Q. Basher[b], F. A. Hamid[b], S. B. A. Hamid[b], E. Omar[b], L. Mohd Salim[b]

[b]Combinatorial Technology and Catalysis Research Centre,

University of Malaya, 50603 Kuala Lumpur, Malaysia

Abstract

This work presents a detailed investigation of the preparation routine for the multi-metal oxide $Mo_1V_{0.30}Te_{0.23}Nb_{0.125}O_x$ used as catalyst for the selective oxidation of propane to acrylic acid. *In-situ* Raman spectroscopy on the initial aqueous polyoxometalate solution prepared from ammonium heptamolybdate, ammonium metavanadate and hexaoxotelluric acid reveals the coexistence of Anderson-type anions $[TeM_6O_{24}]^{n-}$, M=Mo, V; n≥6, and protonated decavanadate species $[H_xV_{10}O_{28}]^{(6-x)-}$. Raman analysis showed that the monomeric motif of the Anderson-type tellurate is preserved after addition of the Nb precursor and the subsequent spray-drying process. Calcination of the X-ray amorphous spray-dried material in air at 548 K seems to be the essential step, leading to a re-arrangement of the tellurate building blocks, generating nanocrystalline precursors of the phases finally established during treatment in helium at 873 K.

Keywords

1. Introduction

Natural gas and petroleum refinery off-gases represent abundant resources of lower alkanes. Recently, much effort has been undertaken to develop novel selective oxidation catalysts that convert these alkanes into more valuable petrochemicals. However, due to the low polarity of the C-H bonds in saturated hydrocarbons, their effective activation is a challenging task. Furthermore, increased reactivity of intermediates like olefins involves the risk of consecutive reactions including C-C bond cleavage or deep oxidation leading to unwanted oxygenates and, finally, to CO_x. In this regard, the direct conversion of propane to acrylic acid has attracted much attention in academic and applied research [1-4]. Molybdenum oxide modified with oxides of vanadium, tellurium and niobium is highly effective in this reaction. As a result of empirical catalyst optimization, acrylic acid yields close to 50% were achieved with a catalyst composed of Mo, V, Te and Nb in the molar ratio 1 : 0.30 : 0.23 : 0.125 [5, 6].

Different phases have been identified to constitute MoVTeNb mixed oxides, including $(Mo_{0.93}V_{0.07})_5O_{14}$, MoO_3 and $TeMo_5O_{16}$ [3, 7]. However, the major focus of attention lies on two structures, originally termed as M1 and M2, respectively, by Ushikubo et al. [8]. Very recently, detailed structural models of the orthorhombic M1 and M2 phase, respectively, have been reported (**Figure 1**) [9]. Using transmission electron microscopy, neutron powder diffraction and synchrotron X-ray powder diffraction, the M1 structure was refined as a mixed metal molybdenum bronze with structural modules similar to the molybdenum sub-oxide Mo_5O_{14} [10]. Sharing corner oxygen atoms, MO_6 octahedra (M = Mo, V) are assembled into layers in the *ab*-plane while hexagonal and heptagonal channels are formed along the *c*-axis by stacking these layers via metal-

Preprint of the Department of Inorganic Chemistry, Fritz-Haber-Institute of the MPG *(for personal use only)* (www.fhi-berlin.mpg.de/ac)

2

oxygen bonds. The channels are partially filled with TeO units. Niobium fully occupies

pentagonal bipyramidal sites. The formula of the refined unit cell has been stated as

$Mo_{7.8}V_{1.2}NbTe_{0.937}O_{28.9}$. The M2 phase is described as an orthorhombic structure with

the formula unit $Mo_{4.31}V_{1.36}Te_{1.81}Nb_{0.33}O_{19.81}$ possessing hexagonal channels only. The

framework octahedra are partially occupied by V and Nb, whereas Te is accommodated

in the channels.

Relations between phase composition and catalytic performance of MoVTeNb mixed

oxides as well as the function of each individual constituent are matters of ongoing

discussions. It has been recently assumed that both phases M1 and M2 could be

involved in the selective oxidation and ammoxidation of propane with M1 being the

catalytically most effective phase for the conversion of propane to acrylonitrile and

acrylic acid, respectively [2]. M2 on its own does not activate propane, but converts

propylene. At high conversions, physical mixtures of the two phases showed symbiosis

in the ammoxidation of propane when brought into intimate contact with each other

[11]. The outstanding catalytic activity of M1 in propane oxidation has been ascribed to

the presence of V^{5+} centers, which are assumed to be absent in M2 [2].

A different approach is based on structural considerations only. Thus, the high

performance of M1 has been attributed to the distortion of the octahedra in the unique

heptagonal arrangement of M1, which might give rise to highly active lattice oxygen

[1]. Ueda et al. demonstrated that catalytic activity can be achieved by hydrothermally

synthesized M1 phase-pure material alone, without the need for any other elements than

Mo and V, although the yield of the orthorhombic M1 phase in the hydrothermal

synthesis of MoV was less than 10% [12]. It appeared that tellurium is not necessarily

required for phase formation, yet, indications have been found that the thermal stability

Preprint of the Department of Inorganic Chemistry, Fritz-Haber-Institute of the MPG *(for personal use only)* (www.fhi-berlin.mpg.de/ac)

3

of the M1 phase is enhanced by addition of Te [1]. Moreover, Te^{4+} was considered to play an important role as active site in the formation of oxygenated products [1]. It was speculated that Te modifies the strength of surface acid sites from strong for deep oxidation to moderate for acrylic acid formation [13]. Tellurium-containing phases have been proposed to be involved in the O-insertion step [14].

The mode of action of niobium has been less thoroughly studied. In general, the selectivity to acrylic acid is increased by niobium addition. Either site isolation effects [15, 16], or an influence of Nb on the morphology and the chemical composition of the catalyst surface [16] have been discussed.

Although, in many cases, the final catalyst has been the object of investigation, the preparation of $MoVTeNbO_x$ catalysts has been studied to a lesser extent. However, the preparation parameters are reported to have a significant effect on the catalytic activity [6, 17]. In the present work we deal with self-assembling processes of polyoxoanions involved in the preparation of a MoVTeNb oxide catalyst in solution. We confined ourselves to the single formulation $Mo_1V_{0.30}Te_{0.23}Nb_{0.125}O_x$, which has been claimed to give the highest yields of acrylic acid in selective propane oxidation [5]. Our aim was to elucidate the impact of chemical reactions in solution on the nature of the dried, calcined and activated material. In the course of the catalyst genesis, formation and rearrangement of molecular building blocks have been monitored by *in-situ* Raman spectroscopy. The bulk structures of precursors and final catalyst were analyzed by X-ray diffraction, while the microstructure was studied by scanning electron microscopy. Options to control and direct the MoVTeNb oxide synthesis will be discussed.

2. Experimental

2.1 Catalyst preparation

$Mo_1V_{0.30}Te_{0.23}Nb_{0.125}O_x$ was prepared according to the method described in the patent literature [18]. The procedure is illustrated in **Scheme 1**. Dissolving 22.53 g ammonium heptamolybdate $(NH_4)_6Mo_7O_{24} \cdot 4\,H_2O$ (AHM) in 100 ml of bidistilled water at 333 K resulted in a colorless solution (pH=5.2) which changed color to yellow after adding 4.49 g ammonium metavanadate $NH_4VO_3 \cdot x\,H_2O$ (AMV). The mixture was heated up to 353 K to form a clear yellow solution (pH=5.5). A deep red solution of pH=5.0 (MoVTe solution) was obtained after adding 6.74 g hexaoxotelluric acid $Te(OH)_6$ at 353 K. Afterwards, the MoVTe solution was cooled down to 313 K. At this temperature, the addition of 7.04 g ammonium niobium oxalate $(NH_4)_2Nb_2(C_2O_4)_5$ dissolved at 296 K in 30 ml bidistilled water (Nb solution, pH=0.8) led to precipitation. An orange slurry was formed (pH=3.2, T=296 K). A Büchi spray dryer B-191 was used to spray-dry this slurry. An inlet temperature of 473 K was chosen. The delivery rate of the pump and the aspirator were attuned to an outlet temperature of 376 K. The resulting spray-dried sample was designated as 349. The spay-dried material was calcined in static air at 548 K (heating rate 10 K/min) for one hour (sample designation 415) and subsequently treated in flowing helium at 873 K (heating rate 2 K/min) for another two hours (sample designation 381).

Separate aqueous solutions of the components added to the initial ammonium heptamolybdate solution were prepared for reference. The concentrations were the same as used for catalyst preparation. Hexaoxotelluric acid and ammonium niobium oxalate were dissolved at 296 K forming colorless solutions of pH=3.7 and 0.8, respectively.

Preprint of the Department of Inorganic Chemistry, Fritz-Haber-Institute of the MPG *(for personal use only)* (www.fhi-berlin.mpg.de/ac)

5

With ammonium metavanadate a light yellow solution of pH=5.7 was obtained at 353 K.

2.2 Catalyst characterization

Raman spectroscopy was performed on a Labram I (Dilor) instrument equipped with a confocal microscope (Olympus). A notch filter (Kaiser Optical) was applied to cut off the laser-line and the Rayleigh scattering up to 150 cm^{-1}. The spectrometer is equipped with a CCD camera (1024*298 diodes), which is Peltier cooled to 243 K to reduce the thermal noise. A HeNe laser (Melles Griot, 15 mW) was used to excite the Raman scattering at 632 nm. For the *in-situ* solution experiments the laser beam was directed through the glass reaction vessel into the solution. The following spectrometer parameters were used: Microscope objective: 10, slit width: 200 μm (spectral resolution: 2.5 cm^{-1}), integration time: 30 s per spectrum and 5 averages. For solution measurements, no power filter was applied. For powders, laser power was reduced to ca. 1 mW at the sample.

Combined thermogravimetric and differential scanning calorimetric analysis (TG-DSC) was performed using an STA 449 C Jupiter apparatus (Netzsch). 48 mg of the spray-dried precursor material were first heated to 548 K at 10 K/min in 100 ml/min of 21% oxygen in nitrogen. After the sample was cooled to room temperature, the gas flow was switched to 100 ml/min Ar and the sample was heated to 873 K at 2 K/min. The gases evolved during thermal analysis were analyzed by transfer through a heated (393 K), fused silica capillary to a Thermostar quadrupole mass spectrometer (Pfeiffer Vacuum).

X-ray diffraction measurements were performed with a STOE STADI-P transmission diffractometer equipped with a focussing primary Ge (111) monochromator and a

position sensitive detector, using Cu-Kα_1 radiation. The program Topas (v.2.1, Bruker AXS) was used to fit the diffraction pattern of the calcined material.

The sample morphology was studied with a Hitachi S-4000 FEG Scanning Electron Microscope (SEM). The micrographs were taken with an accelerating voltage of 5 kV in the SE (Secondary Electron) mode. The EDX (Energy Dispersive X-ray analysis) data were measured with an EDAX Sapphire-detector on an EDAX-DX4 system. The accelerating voltage of the spectra was 25 kV (sample 349) and 15 kV (sample 381), respectively.

3. Results

3.1. Raman spectroscopy on solutions

The low Raman cross-section of water makes Raman spectroscopy a suitable analytical tool for the investigation of inorganic species in aqueous solutions. In order to elucidate chemical processes during the synthesis of the $Mo_1V_{0.30}Te_{0.23}Nb_{0.125}O_x$ catalyst, we monitored the early preparation steps (**Scheme 1**) by *in-situ* Raman spectroscopy.

The Raman spectra of reference solutions are presented in **Figure 2**. When the aqueous ammonium heptamolybdate (AHM) solution is heated up from 333 K (**Figure 2a**) to 353 K (**Figure 2b**), the pH decreases from 5.2 to 5.0. The decrease in pH is accompanied by a partial transformation of ammonium heptamolybdate to ammonium octamolybdate. This pH and temperature dependent process is well known for the given concentration [19] and can be recognized in the Raman spectrum by the appearance of the shoulder at 955 cm^{-1} (**Figure 2b**) [20, 21]. However, heptamolybdate remains the main species at 353 K detectable by its characteristic Mo=O stretching bands at 937 and 893 cm^{-1} (**Figure 2a,b**) [22].

The spectrum of the light yellow ammonium metavanadate (AMV) solution (pH=5.7) at 353 K exhibits a peak at 944 cm^{-1} and a weak shoulder near 900 cm^{-1} (**Figure 2c**). Such bands have been observed with aqueous AMV solutions, albeit, in the pH range from 9.6 to 8 [23]. The peaks were assigned to ν_{VO_2}(sym.) and ν_{VO_2}(as.) modes, respectively, of cyclic $(VO_3)_n^{n-}$ species in which VO_2 units are linked by single oxygen bridges [23].

The spectrum of the colorless solution of hexaoxotelluric acid at 296 K (pH=3.7) shows a single peak at 644 cm^{-1} due to ν(TeO) vibrations [24] (**Figure 2d**).

Bands at 942, 919 and 570 cm^{-1} assigned to Nb=O and Nb-O stretching vibrations, respectively, were observed with the ammonium niobium oxalate solution (pH=0.8, T=296 K) [25] (**Figure 2e**). A summary of Raman bands measured is given in **Table 1**.

Figure 3 shows the Raman spectra of the mixed solutions. When solid AMV is added to the solution of AHM at 353 K (pH= 5.0) the pH increases to 5.5 and significant changes in the Raman spectrum are observed (**Figure 3a**). It is worth mentioning that if one decreases the pH of a pure AMV solution at 353 K with the same concentration as for the binary system from originally 5.7 to 5.5, precipitation occurs. This observation strongly indicates a chemical interaction between AHM and AMV in the mixed solution. However, the presence of bands at 937 and 893 cm^{-1} and the band at 950 cm^{-1} corresponding to heptamolybdate ions and $(VO_3)_n^{n-}$ species, respectively, reveals that the unreacted single Mo and V components still prevail. New bands appear at 980, 956 and 848 cm^{-1}. According to Griffith *et al.*, these bands can be assigned to a decavanadate ion $[V_{10}O_{28}]^{6-}$, which is the main species in aqueous AMV solution at pH around 5.5 [26]. Alternatively the band at 848 cm^{-1}, described as very weak for the decavanadate, may be assigned to asymmetric stretching vibrations of bridging Mo-O-V bonds of a mixed MoV compound.

The subsequent addition of hexaoxotelluric acid at 353 K is accompanied by a pH drop from 5.5 to 5.0 and a color change from light orange to deep red. The Raman spectrum of the ternary MoVTe solution is shown in **Figure 3b**. Bands in the high frequency range are observed at 1000, 937 and 899 cm^{-1}. The band at 1000 cm^{-1} could arise from terminal V=O bonds of protonated decavanadate species $[H_xV_{10}O_{28}]^{(6-x)-}$ [26]. The bands at 937 and 899 cm^{-1} fit very well to the powder Raman spectrum of the Anderson-type heteropolyanion $[TeMo_6O_{24}]^{6-}$ in the form of its ammonium salt [27]. A schematic representation of this anion [28] is given in **Figure 4**. Yuhao *et al.* has synthesized a vanadium substituted heteropolytellurate $(NH_4)_7TeMo_5VO_{24} \cdot 8\,H_2O$ [29]. The replacement of one molybdenum atom in $(NH_4)_6TeMo_6O_{24} \cdot 7\,H_2O$ by vanadium shifted the stretching mode of the terminal M=O bonds from 946 cm^{-1} to 990 cm^{-1} [29]. Taking this into account, the spectral pattern in **Figure 3b** could also be interpreted in terms of the formation of an Anderson-type heteropolytellurate with molybdenum partially replaced by vanadium. Unfortunately the band at 937 cm^{-1} corresponding to the Anderson-type heteropolyanion is at the same position as the most intense band of the heptamolybdate species and, consequently, no statement can be given with respect to possibly remaining non-converted AHM in the ternary MoVTe solution. However, since the band at 644 cm^{-1} due to hexaoxotelluric acid is no longer observed, a quantitative reaction of AHM and an additional incorporation of vanadium into the molybdotellurate seems to be highly probably, because the amount of tellurium added exceeds the Mo : Te stoichiometry in $[TeMo_6O_{24}]^{6-}$.

3.2. Raman spectroscopy on the spray-dried precursor

When finally the strongly acidic (pH=0.8, T=296 K) niobium oxalate solution is added to the ternary mixture of Mo, V and Te at 296 K, the pH drops to 3.2 and a precipitate is

Preprint of the Department of Inorganic Chemistry, Fritz-Haber-Institute of the MPG *(for personal use only)* (www.fhi-berlin.mpg.de/ac)

9

formed after an induction period of several seconds. We were unable to record a Raman spectrum before precipitation occurred. After spray-drying of the gel-like precipitate, a fine orange powder was obtained. For a better comparison of the structural effect of the addition of niobium oxalate to the ternary MoVTe solution, we spray-dried the latter before adding niobium oxalate and plotted the two spray-dried samples together (**Figure 5**). The band pattern of the ternary MoVTe solution (**Figure 3b**) is retained in both spray-dried samples. Interestingly all bands appear much broader after the addition of niobium oxalate.

3.3. Thermal activation

As described in the patent literature, the activation procedure of the $Mo_1V_{0.30}Te_{0.23}Nb_{0.125}O_x$ precursor was carried out in two steps [18]. First, the precursor was calcined in synthetic air at 548 K (heating rate 10 K/min) and held at this temperature for one hour. The resulting material is designated as calcined material. In a subsequent step, the calcined material was heated from room temperature to 873 K with a rate of 2 K/min in helium. The final temperature was maintained for two hours. The obtained material is designated as activated catalyst. We have studied the thermal activation by combined TG-DSC-MS analysis and by X-ray diffraction.

3.3.1. Thermal analysis

During heating in 21% O_2 to 548 K, we can discern four endothermic signals with associated mass losses (**Figure 6**). The first endotherm with a maximum at about 383 K is due to the desorption of water with a mass loss of about 4%. The next two endothermic signals have maxima at 480 and 505 K, and the fourth endothermic signal is a shoulder at about 540 K. Mass spectrometer measurement during the last three endotherms show mass/charge (m/e) signals for 18 (water, when m/e = 18 dominates

Preprint of the Department of Inorganic Chemistry, Fritz-Haber-Institute of the MPG *(for personal use only)* (www.fhi-berlin.mpg.de/ac)

10

over m/e = 17), 17 (NH_3, when 17/18 signal ratio increases), 30 (NO_x), and 44 (CO_2 or perhaps N_2O). The signal for CO_2 (N_2O) shows a maximum or shoulder at each of the last three endotherms. The signal for water has a maximum at 480 K, and the signal for NH_3 reaches a maximum at about 505 K. The NO_x signal is quite broad and cannot be associated with a single endotherm. The mass losses during the last three endotherms total about 17% of the initial mass of the sample.

During the heat treatment in inert gas (**Figure 7**) there are about 4 more steps in weight loss. The first step of about 4% of the initial weight begins at about 500 K, is endothermic, and the gas phase products include m/e 17 and 18 (consistent with H_2O and perhaps some NH_3), m/e 30 (NO_x), and m/e 44 (N_2O or CO_2). The m/e 30 and 44 signals reach maxima at about 560 K, and the m/e 17 and 18 signals reach maxima at 610 K. The next step in mass loss of about 1.4% occurs between about 625 and 660 K, is slightly endothermic, and has a similar gas product makeup with higher levels of m/e 44 and additionally some m/e 28 (N_2). The final two mass loss steps are either slightly endothermic or heat neutral. The mass loss centered at 720 K constitutes 1.7 % of the initial mass and shows gas products with m/e signals of 28 and 44 (N_2 and N_2O). The final mass loss of 1.3% at about 780 K shows no gas phase products. The lack of a signal in the MS indicates that the gas phase products, most likely metal suboxides, condensed before the MS inlet. The last two mass losses do not occur if the sample is heated to 873 K in 21% oxygen (not shown).

3.3.2. X-ray Diffraction

Both the spray-dried precursor (349) and the calcined material (415) are X-ray amorphous, showing only very broad features in the pattern. For the spray-dried precursor 349, these features are located around 11, 27 and 34° 2Θ (**Figure 8a**),

Preprint of the Department of Inorganic Chemistry, Fritz-Haber-Institute of the MPG *(for personal use only)* (www.fhi-berlin.mpg.de/ac)

11

resembling the intensity distribution of reflections found for the crystalline Anderson-type heteropolyanion $(NH_4)_6[TeMo_6O_{24}] \cdot 7H_2O$ (**Figure 8b**) [30]. This observation is in line with the Raman spectroscopic results which document the presence of an Anderson-type anion in the spray-dried precursor. Thus, it seems that no significant changes occur in the local arrangement during the slurry formation and during the spray-drying process compared with the pre-assembled structures in solution. However, the different distribution of features in the XRD pattern of the calcined material 415 (around 8, 26, 34, and 51° 2Θ (**Figure 9a**)) points towards a significant structural rearrangement during the calcination step. The observed intensity distribution is now very similar to the distribution of diffraction peaks found in the final activated material (**Figure 9b**), indicating that the changes during the heat treatment in inert gas are mainly related to the establishment of long range order (crystallization) of the phases already formed during calcination. These assumptions are consistent with the TG-DTA data. The loss of water, ammonia and CO_2/N_2O during calcination goes along with the decomposition of the Anderson-type phase. The final heat treatment in He leads to a material exhibiting a characteristic X-ray diffraction pattern which closely resembles published data [8]. For a more detailed analysis, the diffraction pattern was fitted with structure models of the M1 and M2 phases as published by DeSanto et al. [9] (**Figure 10**). The measured pattern of the activated catalyst (**Figure 10a**) agrees well with the calculated pattern of a mixture of M1 and M2 (**Figure 10b**), showing only minor dicrepancies as visible in the difference (**Figure 10c**). The calculated contributions of the components M1 (**Figure 10d**) and M2 (**Figure 10e**) are shown separately for reference. The XRD fit (**Table 2**) results in a mixture of 60.7 wt.% M1 and 39.3 wt.% M2, corresponding to an average stoichiometry of $Mo_1V_{0.21}Te_{0.22}Nb_{0.11}O_{40.0}$. The

Preprint of the Department of Inorganic Chemistry, Fritz-Haber-Institute of the MPG *(for personal use only)* (www.fhi-berlin.mpg.de/ac)

12

deviation from the nominal stoichiometry $Mo_1V_{0.30}Te_{0.23}Nb_{0.125}O_x$ may result from loss of material due to sublimation during heat treatment or from the presence of amorphous material not detectable by XRD. Moreover, the XRD fit is based on the stoichiometries for M1 and M2 of reference [9], which were obtained for relatively pure phases. The actual stoichiometry of the M1 and M2 phases in our mixture may be different, assuming that the crystal structures allow for some variation in composition, which is hinted by the variations observed in the lattice parameters

3.3.3. Scanning electron microscopy

Figure 11 shows characteristic SEM images of the spray-dried MoVTeNb precursor (349). All particles are spherically shaped with an uneven surface, which contains several types of dents caused by the drying process. The diameter of the mostly hollow particles varies within 1 and 40 μm. Independent of magnification, EDX analysis at different spots exhibits a homogeneous elemental distribution (**Table 3**).

The final activated catalyst (381) (**Figure 12**) consists of particles, which resemble in shape and size very much the particles of the spray-dried precursor (349). However, EDX reveals a more heterogeneous distribution of the elements (**Table 4**). Some spheres are composed of small crystals, which possess a chemical composition close to that of the M1 phase, although the vanadium content is higher (spot 1 and spot 3). These crystals are partly covered by other particles that look like molten material. Elemental analysis of these areas shows a composition close to that of the M2 phase (spot 2). Between the spheres some platelets were found that seem to be a ternary MoVTe compound (spot 4). Crystals of elemental tellurium also were observed (spot 5). The presence of elemental Te in MoVTeNb mixed oxide catalysts has been reported before, e.g. [6].

4. Discussion

When molybdenum oxide is modified with V oxide and minor amounts of Te and Nb oxide, the resulting material attains outstanding catalytic performance in selective oxidation of propane to acrylic acid. The catalytic performance strongly depends on the preparation method applied. The highest yields of acrylic acid have been achieved with catalysts prepared according to the so-called "slurry method" [18]. As described in the experimental section of this paper, this rather complex procedure consists of several steps which are in part highly sensitive to the preparation parameters. First of all, chemical equilibria in the initial polyoxometalate solutions are influenced by temperature, concentration, and pH. Consequently, the nature of isopoly and heteropoly anions formed and the degree of condensation and/or protonation strongly depends on the parameters mentioned. Moreover, it has been reported by Oliver et al. that the pH of the slurry determines the crystallinity and nature of the phases generated in the subsequent thermal treatment [14]. The drying process is critical as well. Lin et al. observed high catalytic activity only after spray-drying [32]. Phase separation tends to occur when other drying techniques were applied, such as freeze-drying. Heating rates, gas composition and flow rates during thermal activation also affect the characteristics of the final product [6]. Therefore, it is not surprising that attempts to reproduce the catalytic benchmarks reported in the patent literature might fail occasionally, a matter of fact that requires systematic inspection of the preparation procedure.

Optimization of the MoVTeNb system can only be achieved, if every single operation is fully understood and its effect on the subsequent operation can be controlled. Recently, such a knowledge based strategy has led to the successful preparation of a $Mo_{0.68}V_{0.23}W_{0.09}O_x$ material, active in the selective oxidation of acrolein to acrylic acid

Preprint of the Department of Inorganic Chemistry, Fritz-Haber-Institute of the MPG *(for personal use only)* (www.fhi-berlin.mpg.de/ac)

14

[31]. This material contains the Mo_5O_{14} structure as the sole crystalline phase. The structural elements of Mo_5O_{14} are very similar to M1, as it is also constituted of pentagonal bipyramides and hexagonal channels [10]. Molybdenum is partially replaced by tungsten in the molybdate units. Vanadyl cations act as linkers between these units. The preparation routine of $Mo_{0.68}V_{0.23}W_{0.09}O_x$ shows striking resemblance to the preparation routine of $MoVTeNbO_X$, such as utilization of AHM as precursor, incorporation of reduction equivalents, spray-drying and calcination in air followed by a final treatment at high temperature in inert gas. While the $Mo_{0.68}V_{0.23}W_{0.09}O_x$ preparation leads to a well defined material that contains a single phase, the $Mo_1V_{0.3}Te_{0.23}Nb_{0.125}O_x$ preparation generally produces a multi-phase catalyst. The present Raman spectroscopic investigations on reference and mixed MoVTe solutions as well as on the spray-dried precursor indicate that parallel formation of various phases seems to be pre-determined by the chemical equilibria in the initial ternary MoVTe solution. The interaction between molybdenum, vanadium and tellurium predominantly leads to the formation of an Anderson-type heteropoly anion $[TeM_6O_{24}]^{n-}$, (M=Mo, V, n≥6). However, vanadium mainly coexists with the Anderson-type heteropoly anion in the form of protonated decavanadates. The addition of niobium oxalate does not change the structure of the polyoxometalate species in solution and also spray-drying preserves the pre-assembled Anderson-type heteropoly anions as observed in the Raman spectrum of the dried material. In accordance with the Raman results, broad reflections were observed by XRD analysis of the spray-dried precursor that are close to the reflections found for the crystalline Anderson-type compound $(NH_4)_6[TeMo_6O_{26}] \cdot 7\,H_2O$ [30]. However, it seems that niobium does affect the crystallinity of the polyoxometalates. It is likely that Nb acts already in the solution as a linker that connects the $[TeM_6O_{24}]^{n-}$

units. The delay of slurry formation after addition of the niobium solution further supports this model. Oliver *et al.* have reported a change in crystallinity of MoVTeNbO catalysts depending on the pH of the slurry [14]. Lowering the pH was assumed to have two effects, first, to decrease the crystallinity of the molybdotellurates formed, and, second, to facilitate the partial introduction of heteroatoms such as V and Nb. The second statement concerning the incorporation of V and Nb may be more important for niobium but seems to be of minor importance for vanadium since the protonated decavanadate is quite stable at low pH [26].

From the above stated coexistence of a variety of different species in solution and in the spray-dried catalyst precursor one can expect that the thermal treatment will not result in a phase-pure material. While the dried precursor is not active in propane oxidation to acrylic acid, stepwise thermal treatment at first in air and then in inert atmosphere activates the catalyst. Crucial seems to be the calcination in air at 548 K that results in dehydration and decomposition of the ammonium salt of the Anderson-type anion $[TeM_6O_{24}]^{n-}$ as clearly shown by TG-DTA-MS analysis. Distinct hints are given by XRD that amorphous precursors of the finally formed crystalline phases are established in this step. The final thermal treatment in inert atmosphere at 873 K obviously consolidates these phases and, concurrently, may cause the formation of minor phases as clearly illustrated by SEM/EDX analysis of the final catalyst. The existence of particles with phase composition different from M1 and M2 is, however, not reflected in the XRD pattern. The formation of minor phases is related to partial vapour phase transport of tellurium and molybdenum oxide at high temperatures in the inert atmosphere. Under these conditions, MoO_3 and Te could be involved in solid-state

Preprint of the Department of Inorganic Chemistry, Fritz-Haber-Institute of the MPG *(for personal use only)* (www.fhi-berlin.mpg.de/ac)

16

redox reactions as described by Bart et al. [33] and may also affect the surface arrangement.

5. Conclusions

It can be concluded from this work that the pre-assembling of polyoxometalates as molecular building blocks of $Mo_1V_{0.30}Te_{0.23}Nb_{0.125}O_x$ can be monitored during catalyst preparation by Raman spectroscopy. The Anderson-type tellurate initially formed in the ternary MoVTe solution is preserved in the spray-dried material. Hence, the role of tellurium in the MoVTeNb synthesis could be described as a structural promoter that arranges molybdenum and tellurium by forming the stable Anderson anion. This close contact of Mo and Te is fundamental for the formation of the required mixed oxide phases during calcination because it presumably prevents the formation of larger amounts of undesirable MoO_2 and MoO_3. However, the Raman spectra have shown that large fractions of vanadium and niobium are not transformed in solution and therefore hinder, after calcination and thermal treatment, the formation of a homogeneous phase composition. Some of the phases observed might be either inactive in partial oxidation of propane, or favor deep oxidation. The contribution of amorphous components existing on top and in between the crystalline particles has to be taken into consideration as well. Therefore, much more room for optimization remains. In fact, a novel strategy for a knowledge based preparation routine is likely to yield better material with increased activity for partial oxidation catalysis. Finally, the stability of a specific phase under reaction conditions must be accounted for and brought into discussion. The particular active phase in the current catalyst system might be the M1 phase as suggested in the literature, however, the fact that this phase is not formed at all in an oxidative atmosphere cast doubts concerning its stability under reaction conditions.

Preprint of the Department of Inorganic Chemistry, Fritz-Haber-Institute of the MPG *(for personal use only)* (www.fhi-berlin.mpg.de/ac)

17

Acknowledgements

Preprint of the Department of Inorganic Chemistry, Fritz-Haber-Institute of the MPG *(for personal use only)* (www.fhi-berlin.mpg.de/ac)

18

6. References

1. D. Vitry, J.-L. Dubois, W. Ueda, J. Mol. Catal. A 220 (2004) 67.

2. R.K. Grasselli, D.J. Buttrey, P. DeSanto, Jr., J.D. Burrington, C.G. Lugmair, A.F. Volpe, Jr., T. Weingand, Catal. Today 91-92 (2004) 251.

3. M. Baca, A. Pigamo, J.-L. Dubois, J.M.M. Millet, Top. Catal. 23 (2003) 39.

4. M.M. Lin, Appl. Catal. A 207 (2001) 1.

5. T. Ushikubo, H. Nakamura, Y. Koyasu, S. Wajiki, US Patent 5 380 933 (1995) to Mitsubishi Kasei Corporation.

6. M.M. Lin, Appl. Catal. A 250 (2003) 305.

7. J.M.L. Nieto, P. Botella, B. Solsona, J.M. Oliver, Catal. Today 81 (2003) 87.

8. T. Ushikubo, K. Oshima, A. Kayou, M. Hatano, Stud. Surf. Sci. Catal. 112 (1997) 473.

9. P. DeSanto, D.J. Buttrey, R.K. Grasselli, C.G. Lugmair, A.F. Volpe, Jr., B.H. Toby, T. Vogt, Z. Kristallogr. 219 (2004) 152.

10. L. Kihlborg, Ark. Kemi 21 (1963) 365, 427; L. Kihlborg, Acta. Chem. Scand. 17 (1963) 1485.

11. J. Holmberg, R.K. Grasselli, A. Andersson, Appl. Cata. A. 270 (2004) 121.

12. T. Katou, D. Vitry, W. Ueda, Chem. Lett. 32 (2003) 1028.

13. T. Katou, D. Vitry, W. Ueda, Catal. Today 91-92 (2004) 237.

14. J.M. Oliver, J.M.L. Nieto, P. Botella, A. Mifsud, Appl. Catal. A 257 (2004) 67.

15. R.K. Grasselli, J.D. Burrington, D.J. Buttrey, P. DeSanto, Jr., C.G. Lugmair, A.F. Volpe, Jr., T. Weingand, Top. Catal. 23 (2003) 5.

16. D. Vitry, Y. Morikawa, J.L. Dubois, W. Ueda, Appl. Catal. A 251 (2003) 411.

17. H. Tsuji, Y. Koyasu, J. Amer. Chem. Soc. 124 (2002) 5608.

Preprint of the Department of Inorganic Chemistry, Fritz-Haber-Institute of the MPG *(for personal use only)* (www.fhi-berlin.mpg.de/ac)

19

18. T. Ushikubo, I. Sawaki, K. Oshima, K. Inumaru, S. Kobayakawa, K. Kiyono, US Patent 5 422 328 (1995) to Mitsubishi Kasei Corporation.

19. M.T. Pope, Heteropoly and Isopoly Oxometalates, Springer Verlag, Berlin, 1983, p.42.

20. J. Aveston, E. W. Anacker, J.S. Johnson, Inorg. Chem. 3 (1964) 735.

21. G. Mestl, T.K.K. Srinivasan, Catal. Rev.-Sci. Eng. 40 (1998) 451.

22. K.-H. Tytko, B. Schönfeld, Z. Naturforsch. B 30 (1975) 471.

23. W.P. Griffith, T.D. Wickins, J. Chem. Soc. (A) (1966) 1087.

24. J. Gupta, Nature 140 (1937) 685; H.Siebert, Z. anorg. Allg. Chemie 301 (1959) 11.

25. Jih-Mirn Jehng, I.E. Wachs, J. Raman Spectrosc. 22 (1991) 83.

26. W.P. Griffith, P.J.B. Lesniak, J. Chem. Soc. (A) (1969) 1066.

27. I.L. Botto, C.I. Cabello, H.J. Thomas, Mater. Chem. Phys. 47 (1997) 37.

28. J.S. Anderson, Nature, 140 (1937) 850.

29. S. Yuhao, L. Jingfu, W. Enbo, Inorg. Chim. Acta 117 (1986) 23.

30. H.T. Evans, Jr., J. Amer. Chem. Soc. 90 (1968) 3275.

31. S. Knobl, G.A. Zenkovets, G.N. Kryukova, O. Ovsitser, D. Niemeyer, R. Schlögl, G. Mestl, J. Catal. 215 (2003) 177.

32. M.M. Lin, Appl. Catal. A 250 (2003) 287.

33. J.C.J. Bart, G. Petrini, N. Giordano, Z. anorg. Allg. Chem. 413 (1979) 180.

Preprint of the Department of Inorganic Chemistry, Fritz-Haber-Institute of the MPG *(for personal use only)* (www.fhi-berlin.mpg.de/ac)

20

Table 1

Raman band positions measured in aqueous solutions

solution	T [K]	pH	ν [cm^{-1}] [a]	assignment	reference
AHM	333	5.2	937 (s) 893 (m)	ν (Mo=O) $Mo_7O_{24}^{6-}$	23
AHM	353	5.0	955 (sh)	ν (Mo=O) $Mo_8O_{26}^{4-}$	21-23
AMV	353	5.7	944 (s) 900 (sh)	ν (V=O) $[VO_3]_n^{n-}$	24
Te(OH)$_6$	296	3.7	644 (s)	ν (Te-O)	25
ANO[b]	296	0.8	570 (m) 942 (s) 919 (s)	ν (Nb-O) ν (Nb=O)	26
AHM + AMV	353	5.5	980 (s) 956 (m) 848 (m)	ν (V=O) $[V_{10}O_{28}]^{6-}$ ν (V-O-V) or ν (Mo-O-V)	27
AHM + AMV + Te(OH)$_6$	353	5.0	1000 (m) 975 (vw) 937 (s) 899 (m)	ν (V=O) $[H_xV_{10}O_{28}]^{(6-x)-}$ or ν (M=O) $[TeMo_5VO_{24}]^{7-}$ ν (Mo=O) $[TeMo_6O_{24}]^{6-}$	27 29 28

[a]s = strong, m = medium, w = weak, vw = very weak, sh = shoulder

[b]ANO = ammonium niobium oxalate

Table 2

Lattice parameters obtained from the XRD fit

	a [Å]	b [Å]	c [Å]
M1	21.1439(15)	26.5896(18)	4.0131(3)
M2	12.6449(19)	7.2984(14)	4.02060(16)

Preprint of the Department of Inorganic Chemistry, Fritz-Haber-Institute of the MPG *(for personal use only)* (www.fhi-berlin.mpg.de/ac)

21

$(NH_4)_6Mo_7O_{24} \cdot 4\ H_2O$ (0.126 mol Mo) / 100 ml H_2O

T = 353 K / pH = 5.0

$NH_4VO_3 \cdot x\ H_2O$

(0.038 mol V, powder)

$MoV_{0.30}$

T = 353 K / pH = 5.5

$Te(OH)_6$ (0.029 mol Te, powder)

$MoV_{0.30}Te_{0.23}$

T = 353 K / pH = 5.0

cool down to 313 K

$(NH_4)_2Nb_2(C_2O_4)_5 \cdot x\ H_2O$ (0.016 mol Nb) /

30 ml H_2O / T = 296 K / pH = 0.8

$MoV_{0.30}Te_{0.23}Nb_{0.13}$

(slurry)

T = 296 K / pH = 3.2

spray-drying

$MoV_{0.30}Te_{0.23}Nb_{0.13}$

(spray-dried (349))

548 K (10 K/min) / 1 h / static

$MoV_{0.30}Te_{0.23}Nb_{0.13}$

(calcined (415))

873 K (2 K/min) /

2 h / He flow

$MoV_{0.30}Te_{0.23}Nb_{0.13}$

(activated (381))

Scheme 1. Preparation steps and critical parameters.

A

B
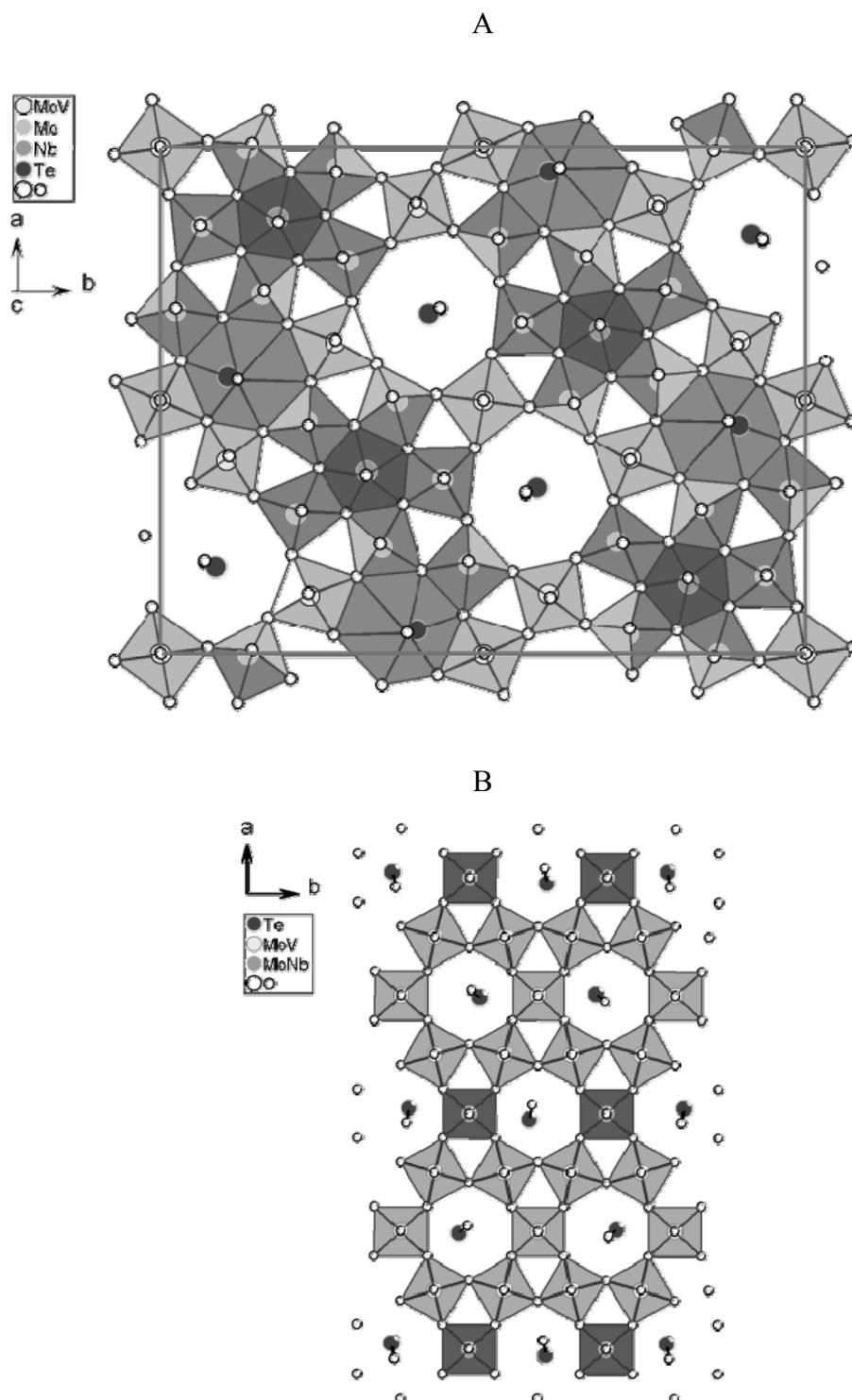
Figure 1. Schematic representation of the refined structural models (A) of the M1 phase
($Mo_{7.8}V_{1.2}NbTe_{0.937}O_{28.9}$) and (B) of the M2 phase ($Mo_{4.31}V_{1.36}Nb_{0.33}Te_{1.81}O_{19.81}$) as 2 x
2 unit cell model, respectively, according to [9].

Preprint of the Department of Inorganic Chemistry, Fritz-Haber-Institute of the MPG *(for personal use only)* (www.fhi-berlin.mpg.de/ac)

24
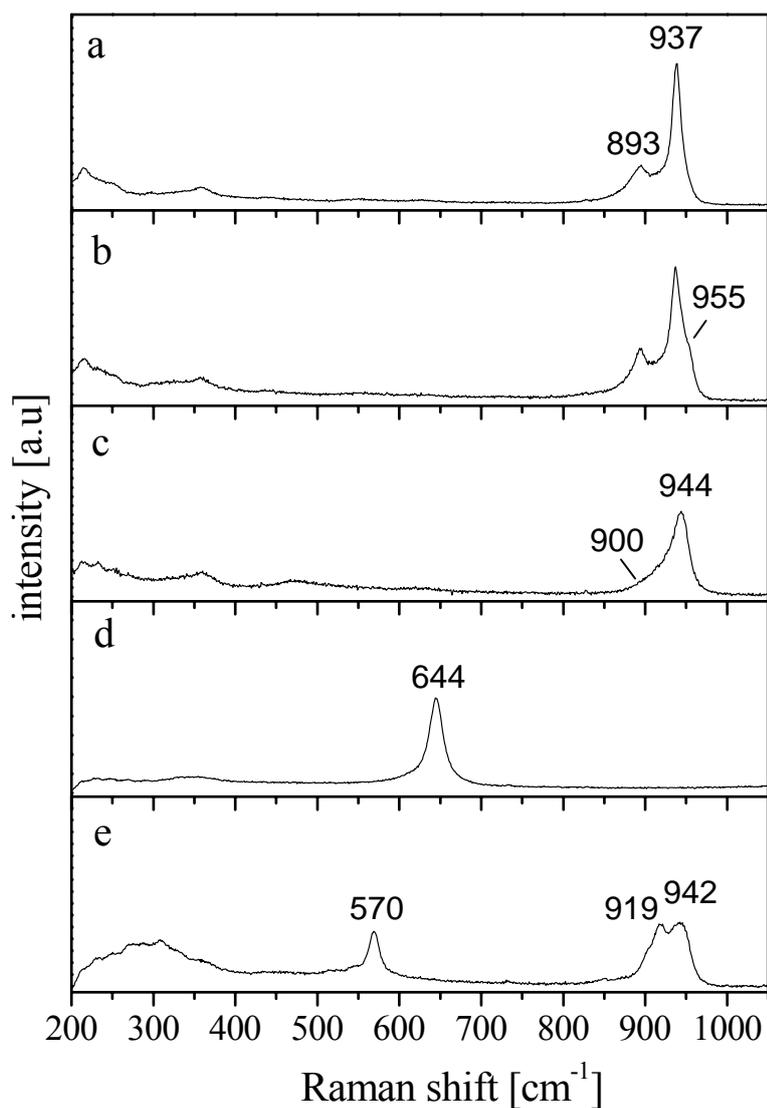
Figure 2. *In-situ* Raman spectra of aqueous solutions of a) AHM (pH=5.2, T=333 K), b) AHM (pH=5.0, T=353 K), c) AMV (pH=5.7, T=333 K), d) $Te(OH)_6$ (pH=3.7, T=296 K) and e) $(NH_4)_2Nb_2(C_2O_4)_5$ (pH=0.8, T=296 K).
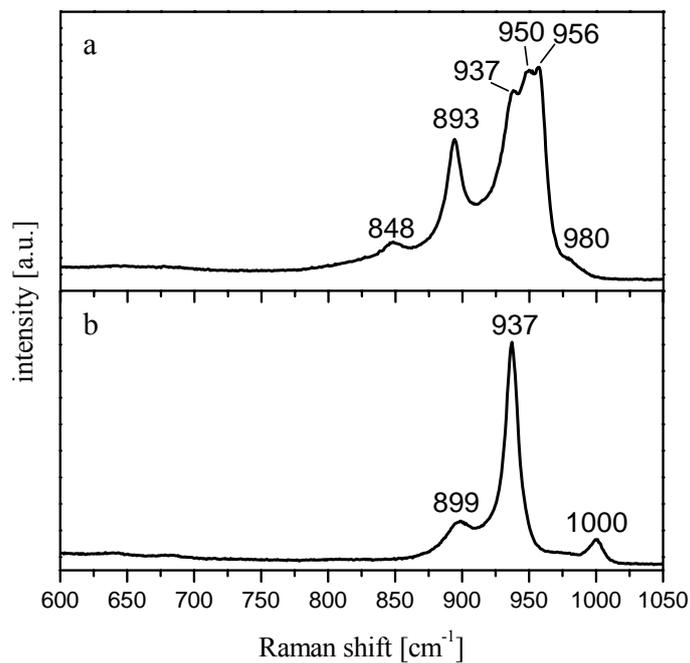
Figure 3. *In-situ* Raman spectra of a) the binary MoV solution (pH=5.5, T=353 K) and b) the ternary MoVTe solution (pH=5.0, T=353 K).
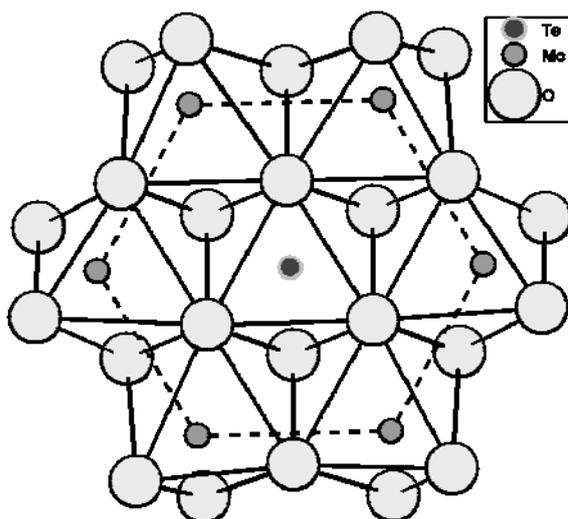
**Figure 4.** Schematic representation of the Anderson-type anion $[Mo_6TeO_{24}]^{6-}$.
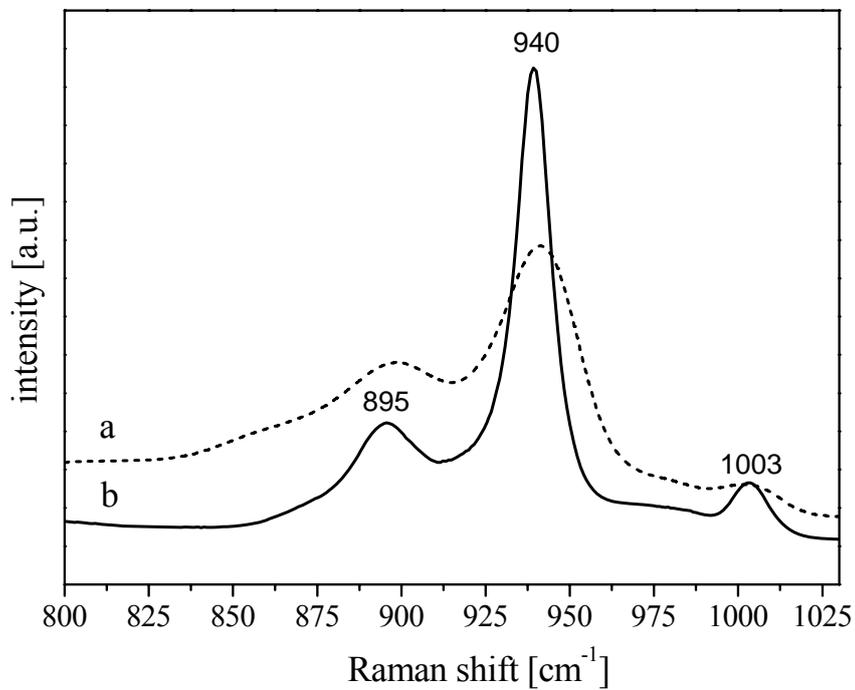
Figure 5. Raman spectra of the spray-dried precursors a) MoVTeNb and b) MoVTe.
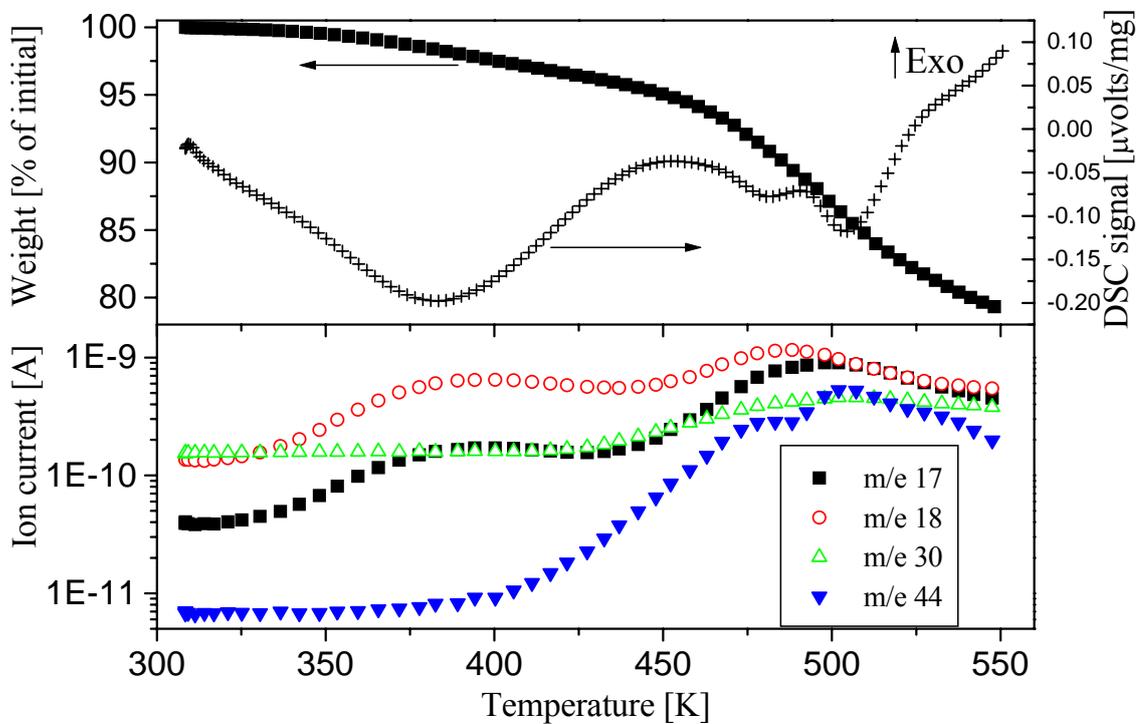
**Figure 6.** Calcination in synthetic air: TG / DSC curves (top); MS signal of mass 17, 18, 30 and 44 (bottom).

Preprint of the Department of Inorganic Chemistry, Fritz-Haber-Institute of the MPG *(for personal use only)* (www.fhi-berlin.mpg.de/ac)

28
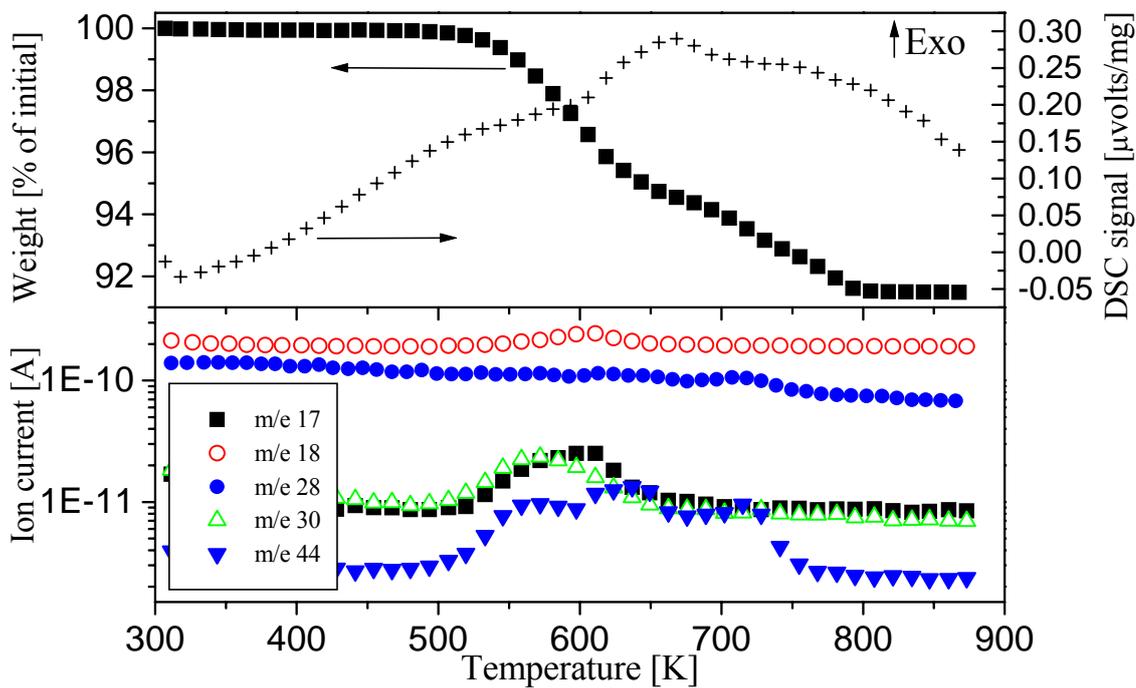
Figure 7. Heat treatment in argon: TG / DSC curves (top); MS signal of mass 17, 18, 28, 30 and 44 (bottom).

Preprint of the Department of Inorganic Chemistry, Fritz-Haber-Institute of the MPG *(for personal use only)* (www.fhi-berlin.mpg.de/ac)

29
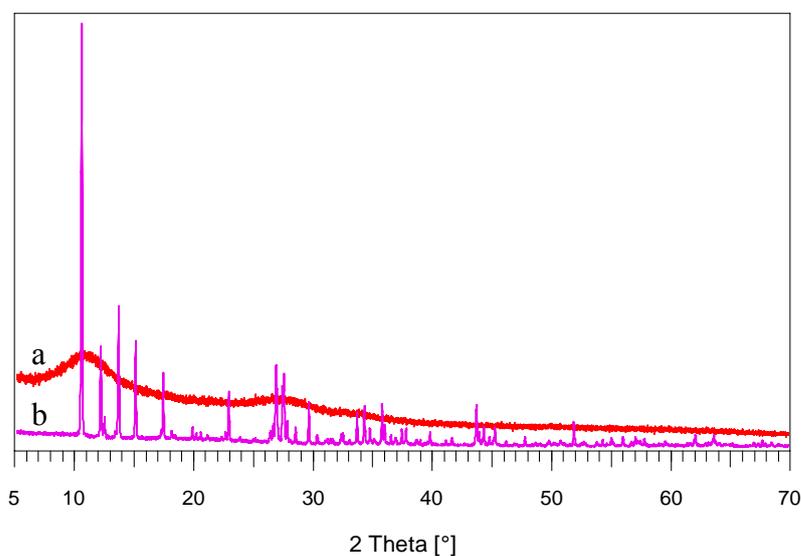
Figure 8. XRD patterns of a) the spray-dried precursor 349 and b) crystalline $(NH_4)_6[TeMo_6O_{24}] \cdot 7\ H_2O$.
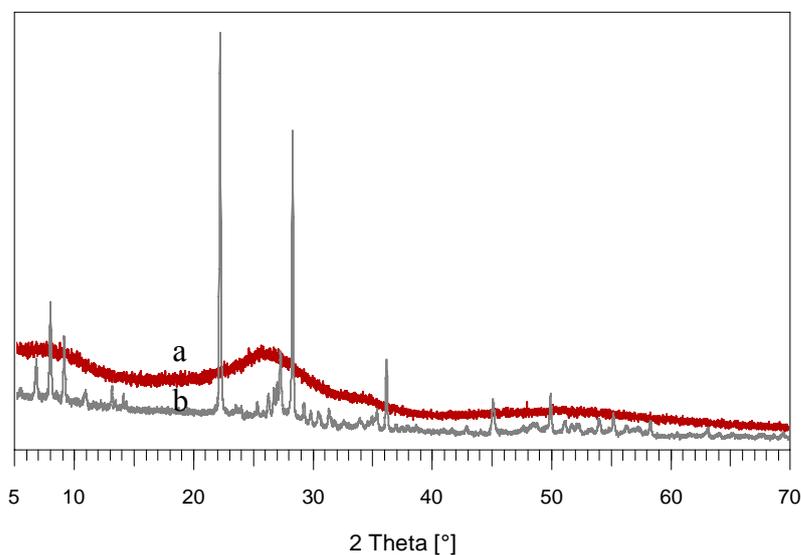

**Figure 9.** XRD patterns of a) the calcined material 415 and b) the activated catalyst 381.
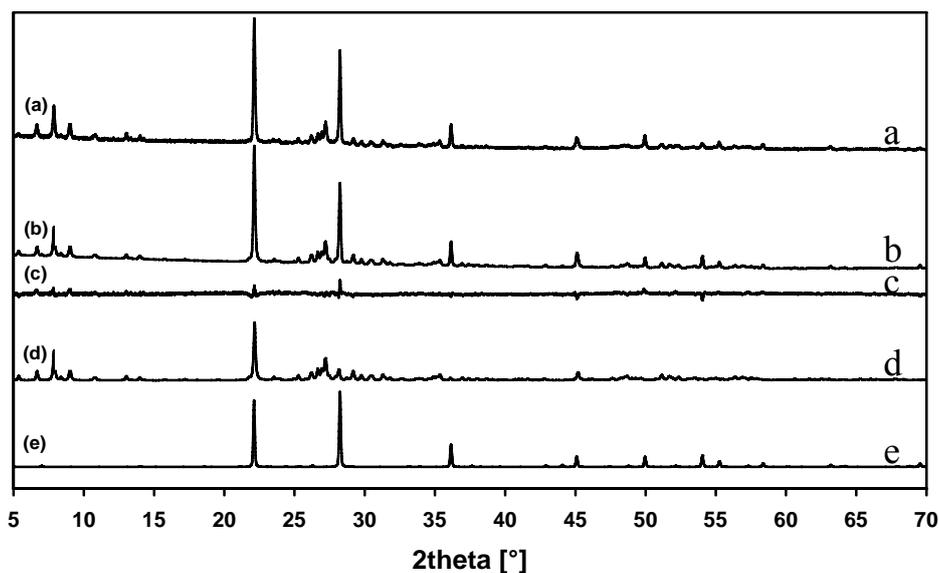
Figure 10. Comparison of a) measured pattern of the activated catalyst 381, b) calculated pattern (mixture of 60% M1 and 40% M2), c) difference a-b and calculated contributions of the components d) M1 and e) M2.
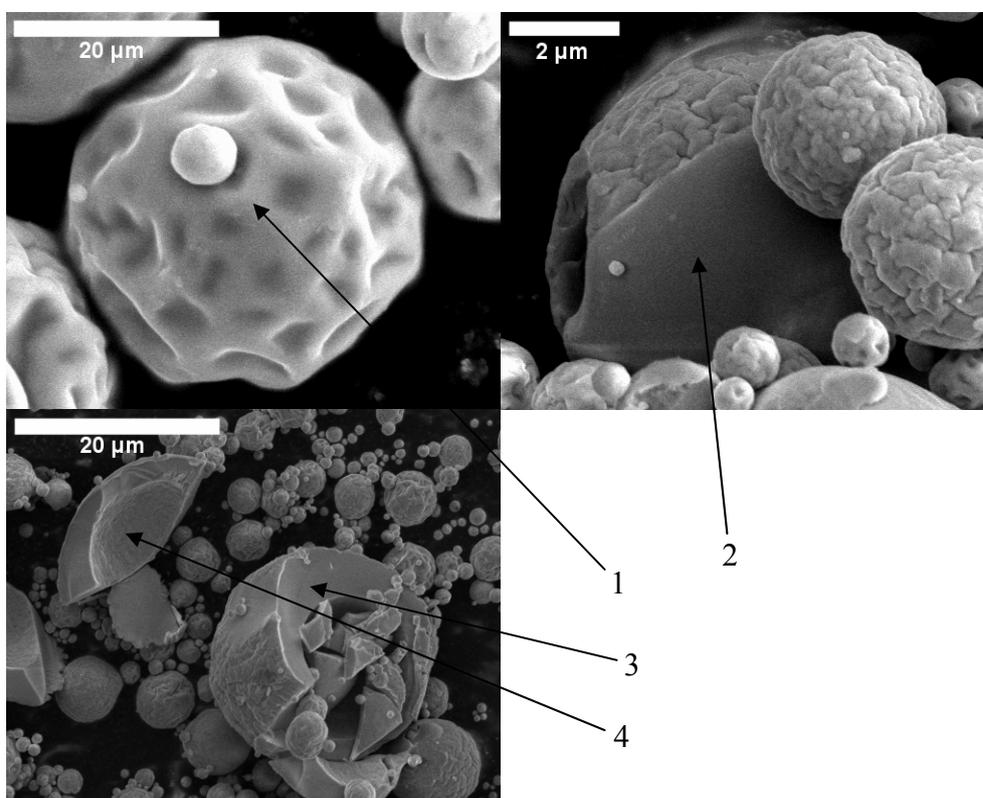

Figure 11. SEM pictures of representative particles of the spray-dried MoVTeNb precursor (349). For results of EDX analysis at the spots indicated see **Table 3**.

Preprint of the Department of Inorganic Chemistry, Fritz-Haber-Institute of the MPG *(for personal use only)* (www.fhi-berlin.mpg.de/ac)

31
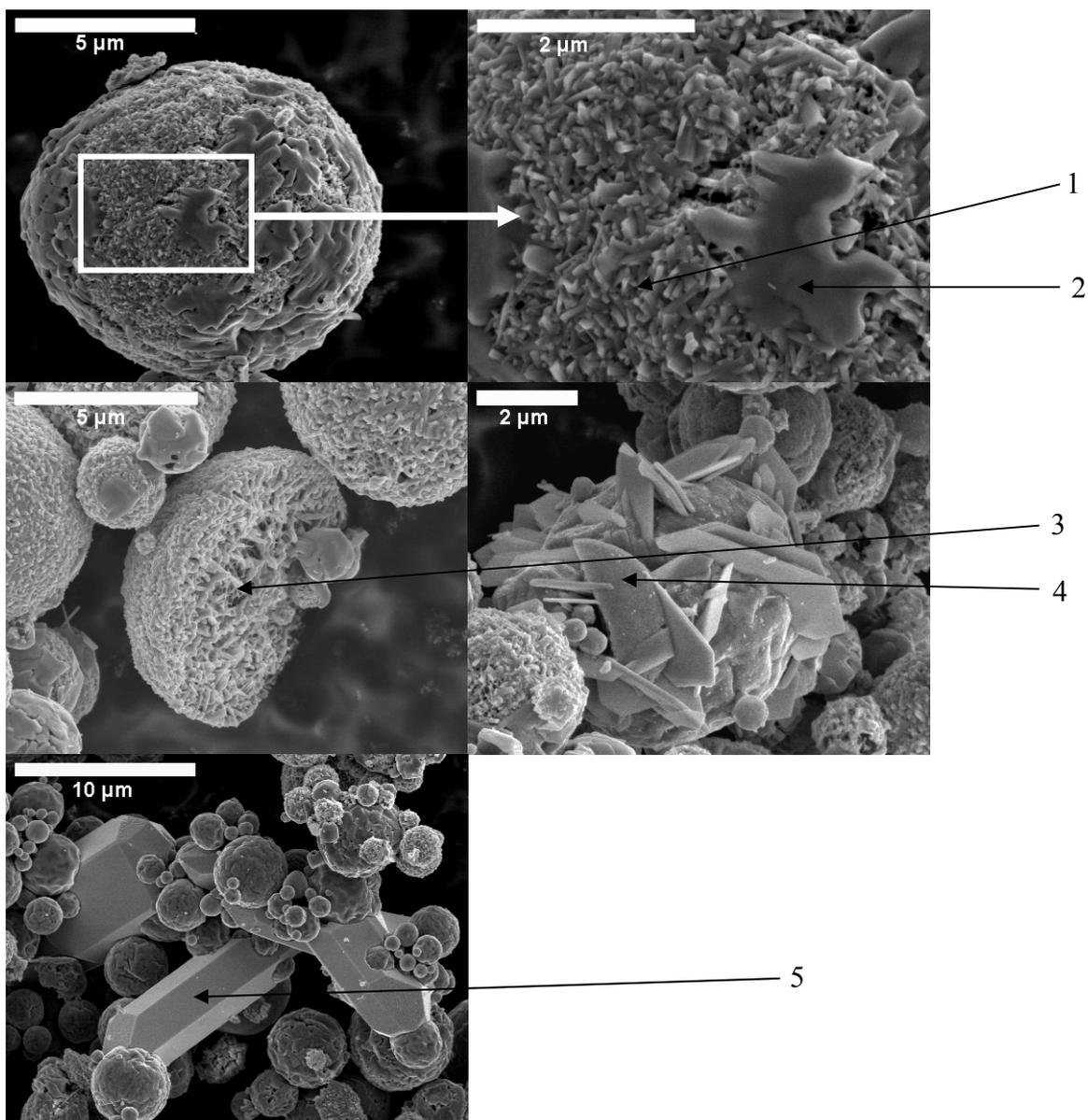
Figure 12. SEM pictures of representative particles of the final catalyst (381). For results of EDX analysis at the spots indicated see **Table 4**.

Preprint of the Department of Inorganic Chemistry, Fritz-Haber-Institute of the MPG *(for personal use only)* (www.fhi-berlin.mpg.de/ac)

32